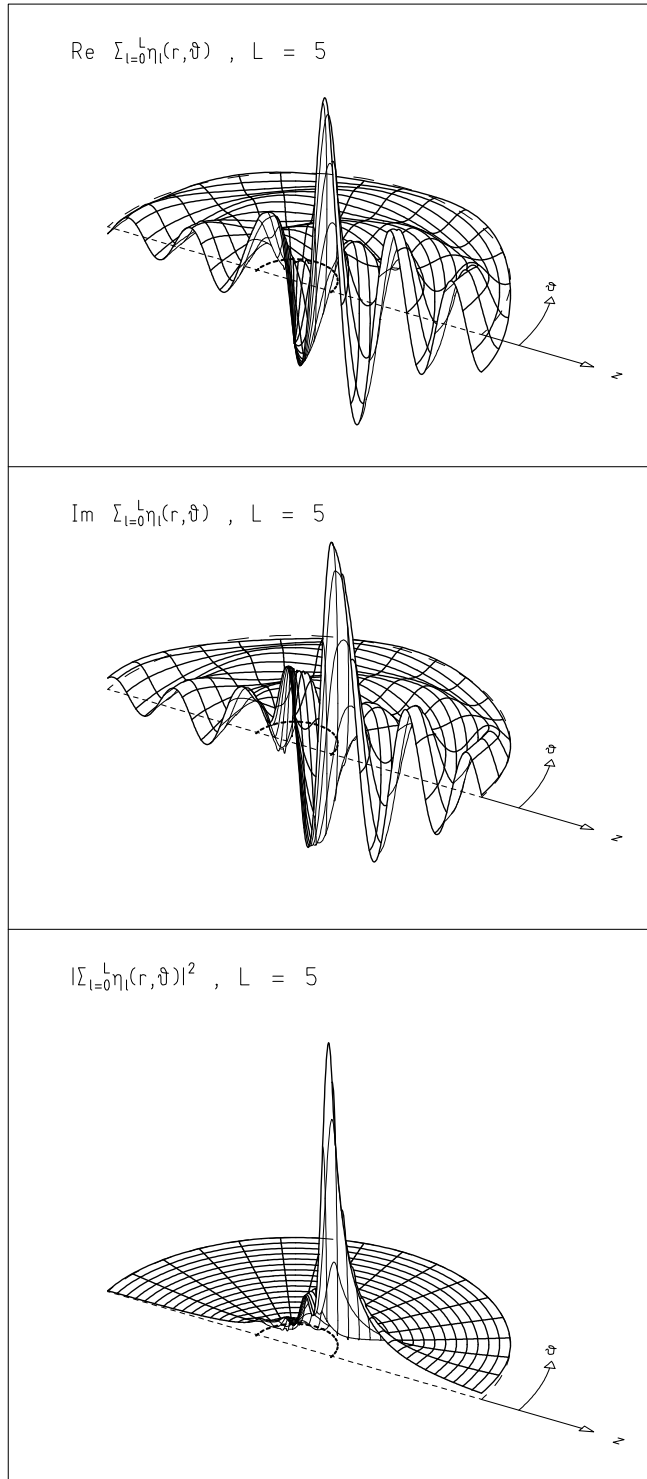
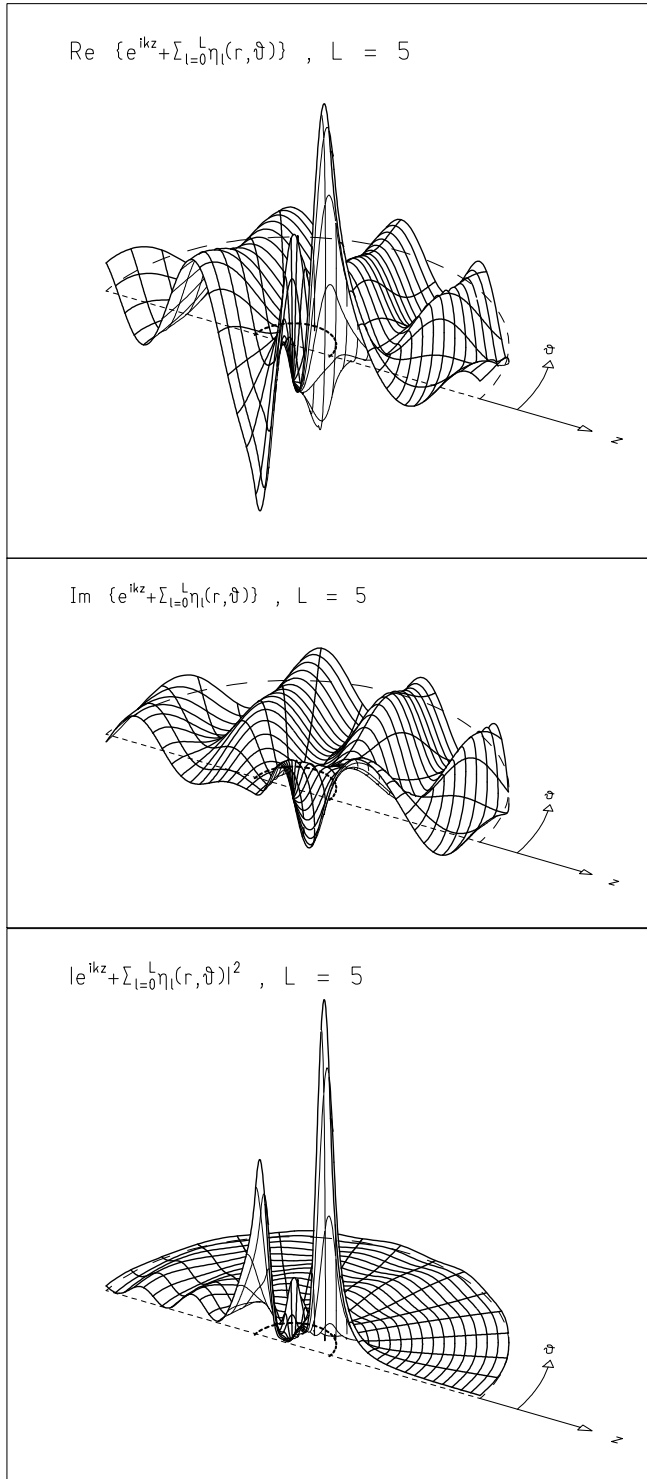


Fig. 15.1. Scattering of a plane wave incident from the left along the  $z$  direction by an attractive potential. The potential is confined to region  $r < d$  indicated by the small half-circle. Shown are the real part, the imaginary part, and the absolute square of the wave function  $\varphi_k^{(+)}$ . The figure corresponds exactly to the situation of Figure 12.1, except for the change  $V_0 \rightarrow -V_0$  in the scattering potential.



**Fig. 15.2.** Real part, imaginary part, and absolute square of the scattered spherical wave  $\eta_k$  resulting from the scattering of a plane wave by an attractive potential, as shown in Figure 15.1.



**Fig. 15.3.** Real part, imaginary part, and absolute square of the wave function  $\varphi_{\mathbf{k}}^{(+)}$  for the scattering of a plane wave by an attractive potential as given in Figure 15.1, but for a resonance energy  $E = E_{\text{res}}$  of the wave.

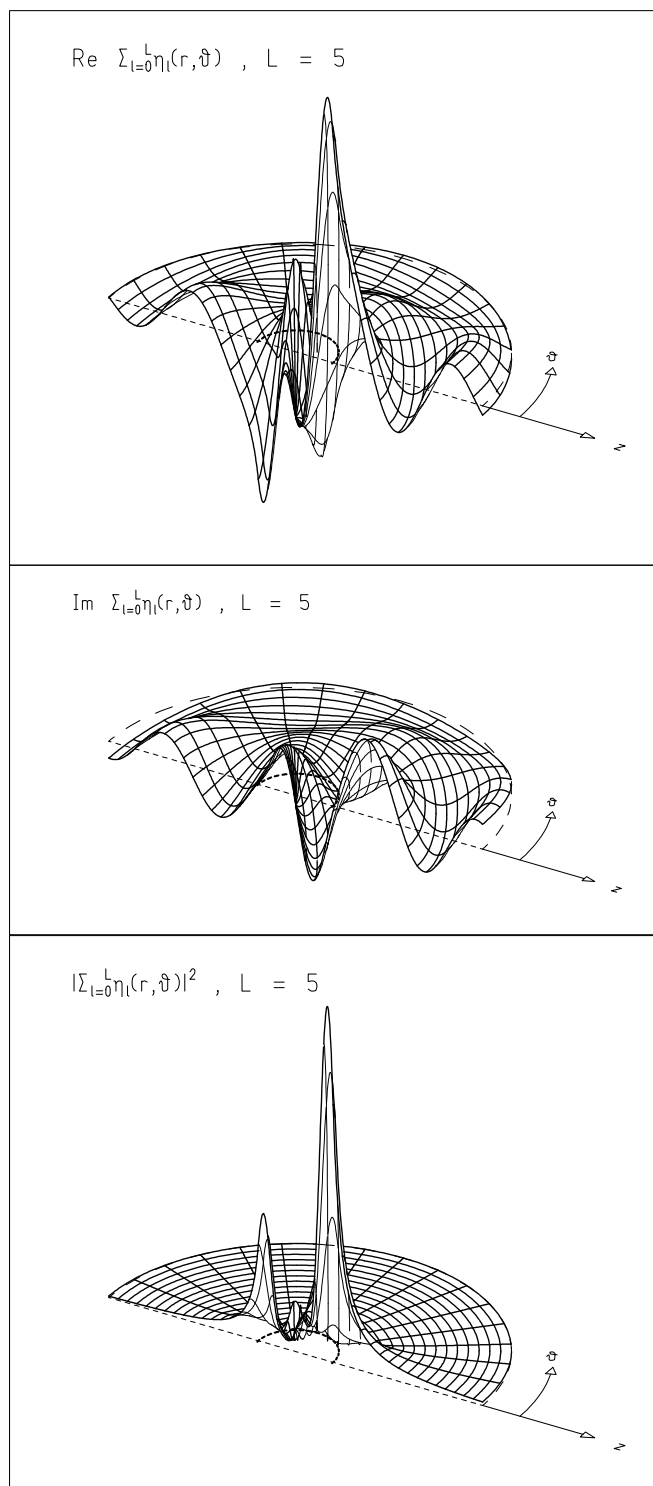


**Fig. 15.4.** Real part, imaginary part, and absolute square of the scattered spherical wave  $\eta_k$  resulting from the scattering of a plane wave of resonance energy  $E = E_{\text{res}}$  by the same attractive potential as in Figure 15.3.

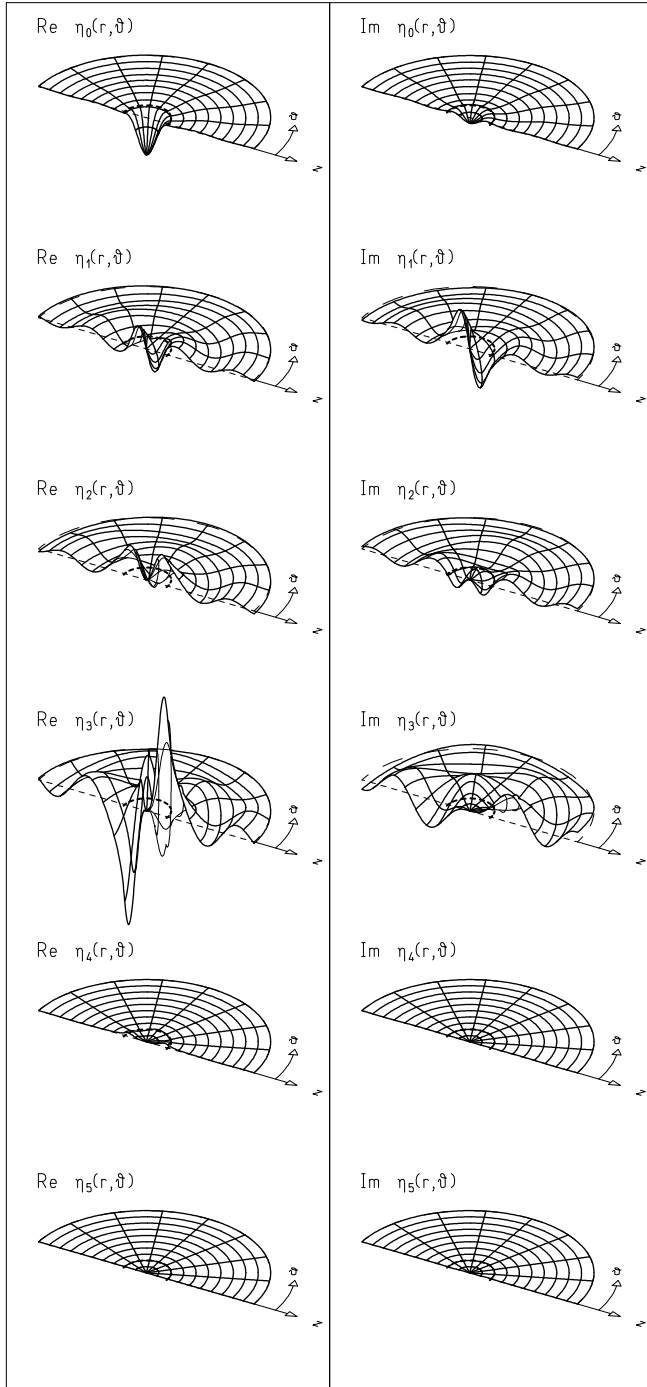


**Fig. 15.5.** Real and imaginary parts of the scattered partial waves  $\eta_\ell$  resulting from the scattering of a plane wave of resonance energy  $E = E_{\text{res}}$  by the attractive potential as in Figures 15.3 and 15.4. The resonance is in the partial wave for  $\ell = 3$ .

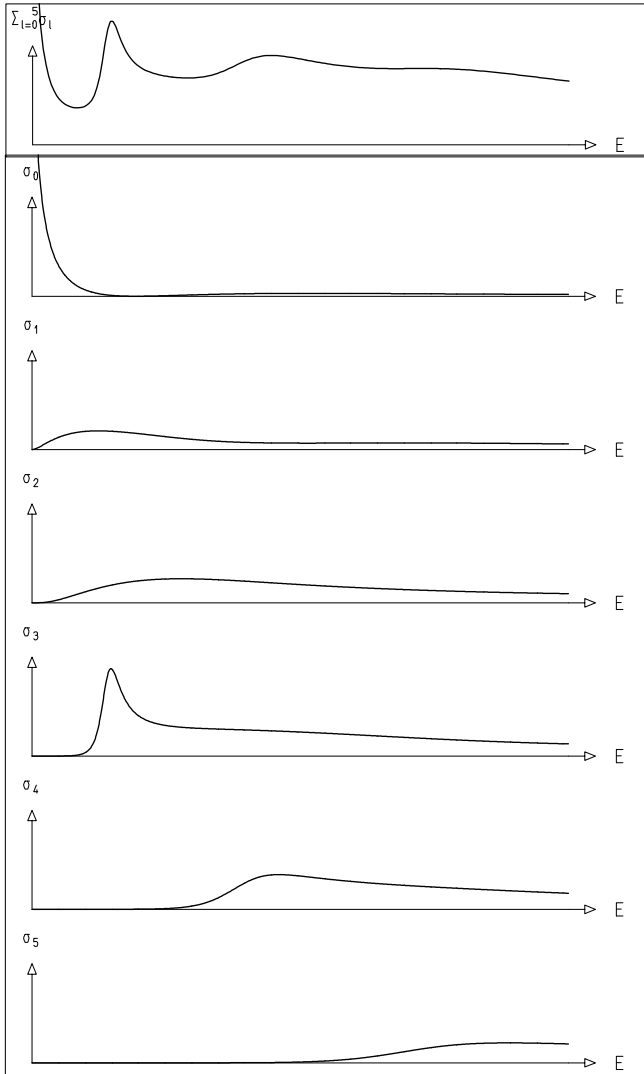


**Fig. 15.6.** The partial cross sections  $\sigma_\ell(E)$  and the total cross section  $\sigma_{\text{tot}}(E)$  approximated by the sum over the first few partial cross sections for the scattering of a plane wave of energy  $E$  by the attractive potential used in Figures 15.1 through 15.5. For resonant energy  $E = E_{\text{res}}$  there is a sharp maximum in  $\sigma_3$  which is reflected in  $\sigma_{\text{tot}}$  approximated by the sum over the first six partial cross sections and shown in the top diagram of the figure.

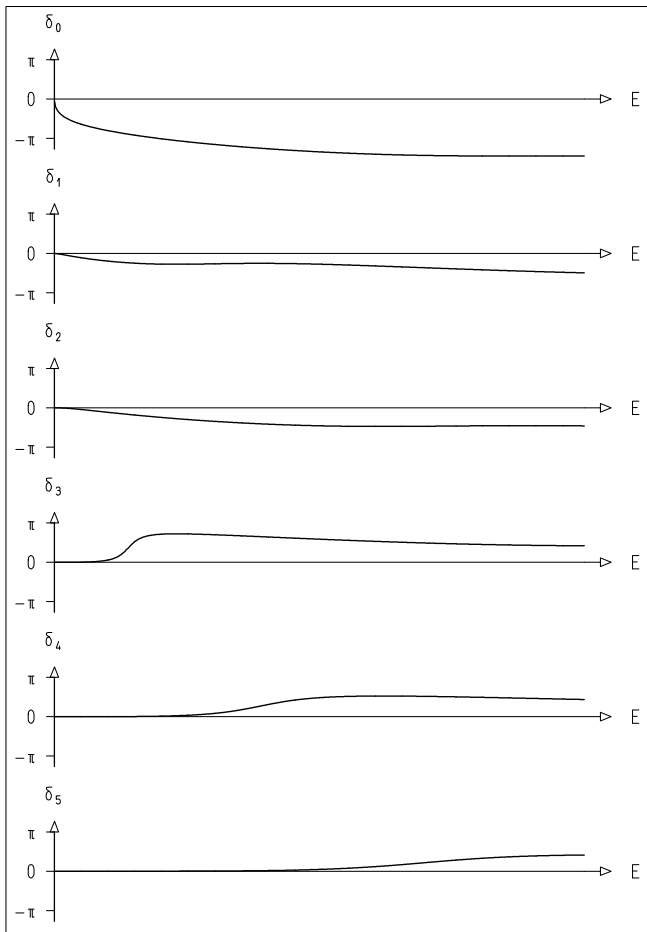


**Fig. 15.7.** The phase shifts  $\delta_\ell(E)$  for the situation of Figure 15.6. For  $E = 0$  we put  $\delta_\ell(0) = 0$ . All phase shifts except  $\delta_3$  vary only slowly with energy. Near  $E = E_{\text{res}}$  the phase shift  $\delta_3(E)$  rises sharply, passing through  $\delta_3(E = E_{\text{res}}) = \pi/2$ , see also the bottom right diagram in Figure 15.8.

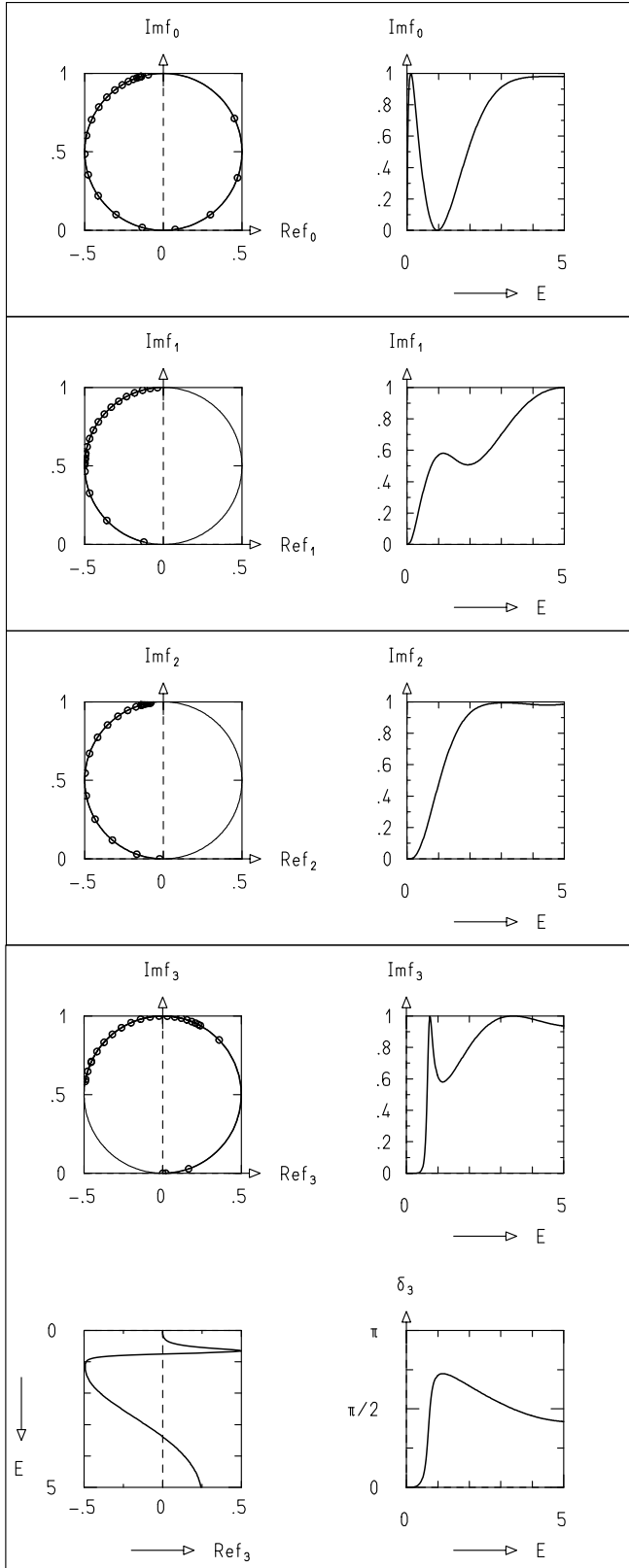


**Fig. 15.8.** Argand diagrams, that is, diagrams of the energy dependence of the complex partial scattering amplitudes  $f_\ell(E)$ , for the scattering of a plane wave of energy  $E$  by the attractive potential used in Figures 15.1 through 15.7 for  $\ell = 0, 1, 2, 3$ . The amplitude  $f_\ell$  moves on a circle in the complex plane. Small circles are placed on the circle at points equidistant in energy. For the nonresonant partial waves,  $\ell = 0, 1, 2$ , only the Argand diagram itself and its projection on the  $\text{Im} f_\ell, E$  plane are shown. The function  $\text{Im} f_\ell(E)$  is closely related to the partial cross section  $\sigma_\ell(E)$ . For resonant wave  $\ell = 3$  both  $\text{Im} f_\ell(E)$  and  $\text{Re} f_\ell(E)$  projections and the phase shift  $\delta_3(E)$  are shown. Near resonance energy  $E = E_{\text{res}}$  the partial scattering amplitude  $f_3(E)$  performs a swift counterclockwise motion through point  $(0, 1)$  in the complex plane, giving rise to (1) the pronounced maximum in  $\text{Im} f_3(E_{\text{res}})$ , (2) the steep drop of  $\text{Re} f_3(E)$  through  $\text{Re} f_3(E_{\text{res}}) = 0$ , and (3) the sharp rise of  $\delta_3(E)$  through  $\delta_3(E_{\text{res}}) = \pi/2$ .



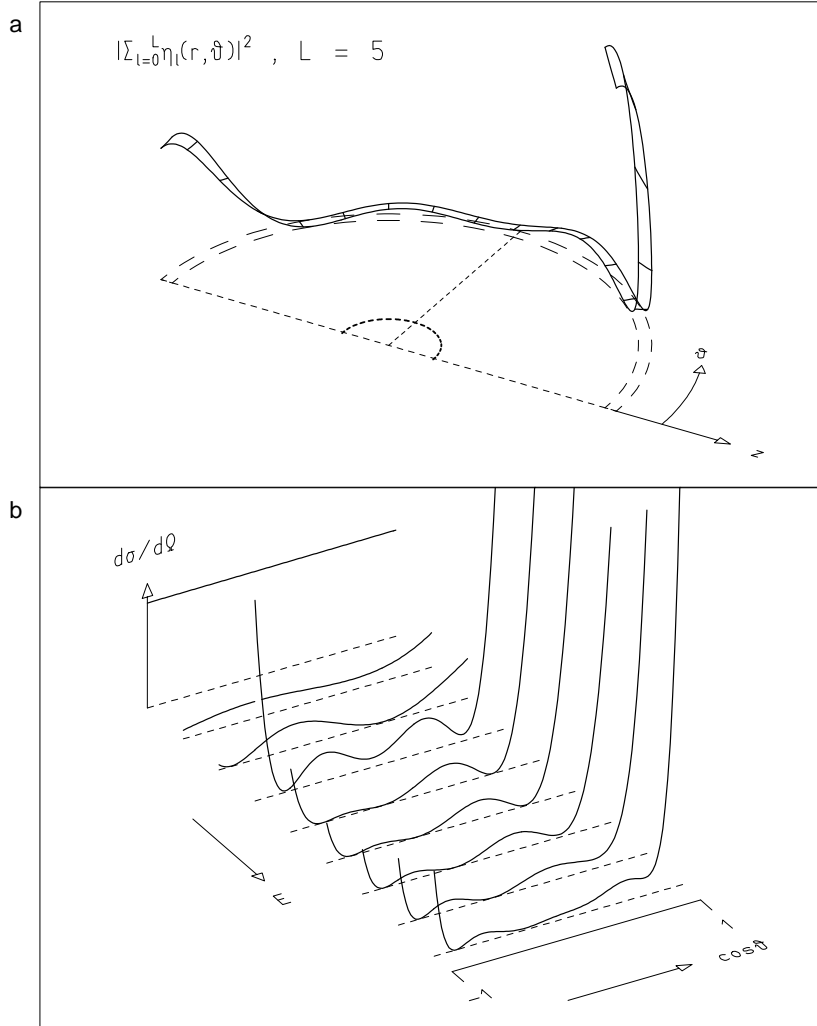


Fig. 15.9. (a) Intensity of the scattered spherical wave resulting from the scattering of a plane wave incident in the  $z$  direction onto an attractive potential restricted to a small region  $r < d$ , indicated by the small dashed half-circle. The intensity far outside the potential region is a function of the scattering angle  $\vartheta$ . The energy of the incident wave is the resonance energy  $E = E_{\text{res}}$ . (b) Energy dependence of the differential scattering cross section  $d\sigma/d\Omega$  shown over a linear scale in  $\cos \vartheta$ . The differential cross section is constant in  $\cos \vartheta$ , indicating isotropic scattering, for  $E \approx 0$  (background). At resonance energy  $E = E_{\text{res}}$  (fourth line from the back) it is given approximately by the square of the Legendre polynomial  $P_3(\cos \vartheta)$ , since the partial scattering amplitude  $f_3$  dominates the cross section.

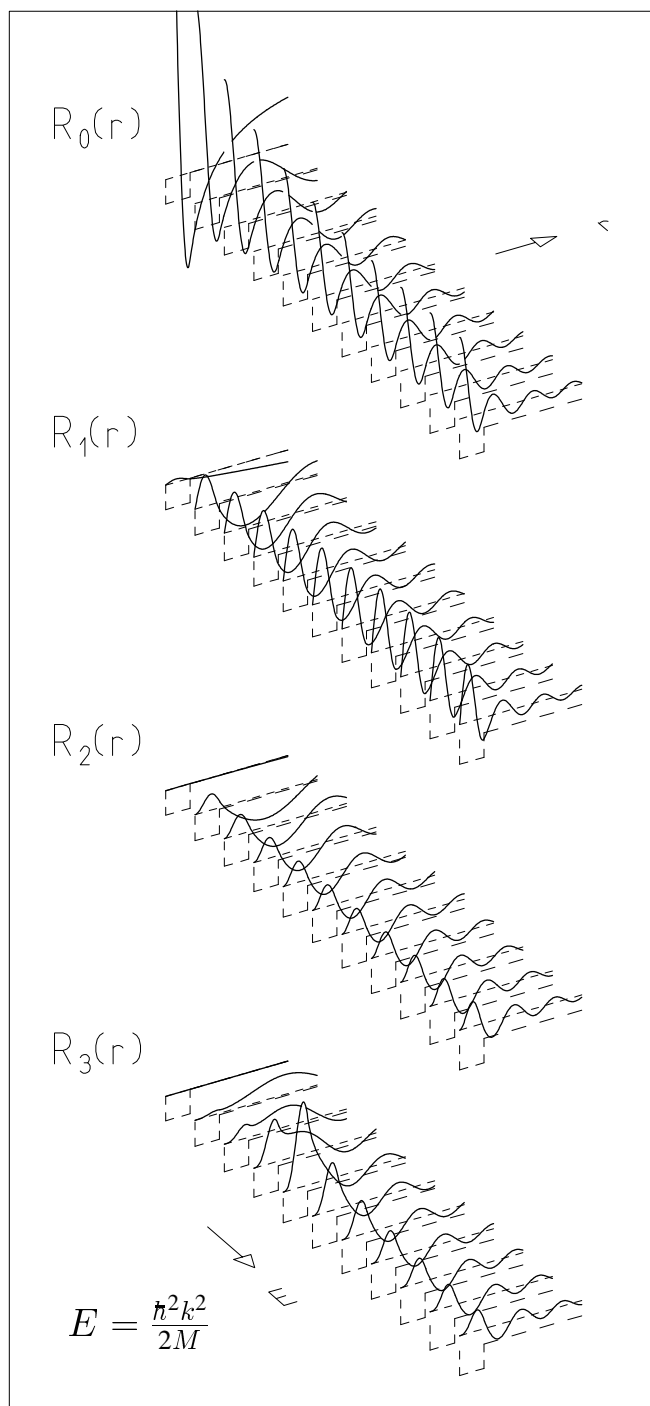
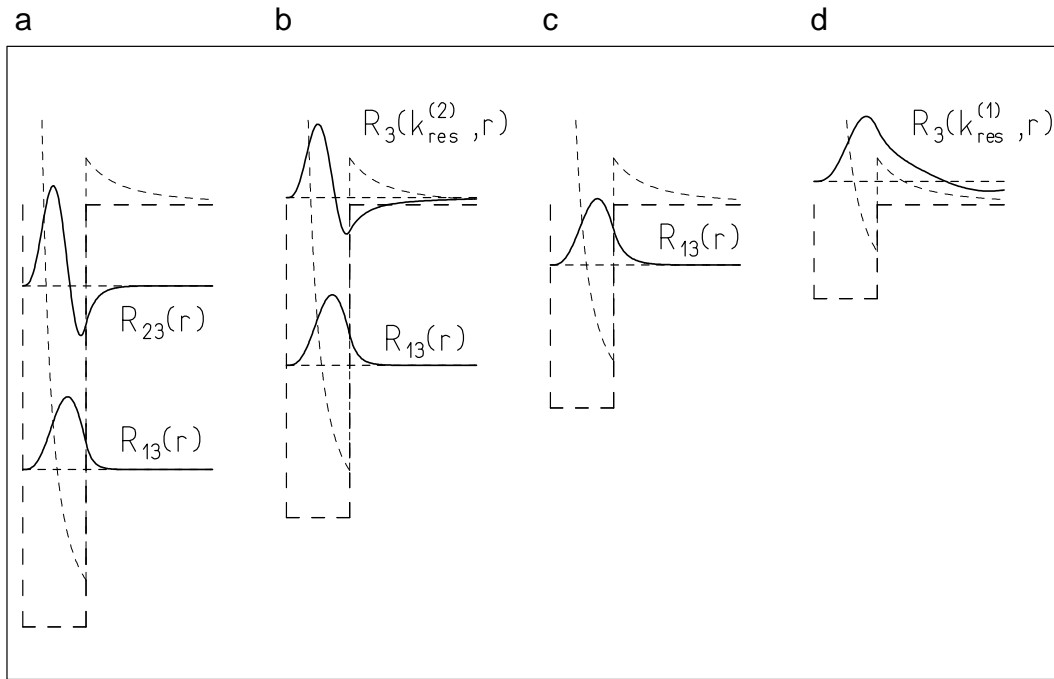
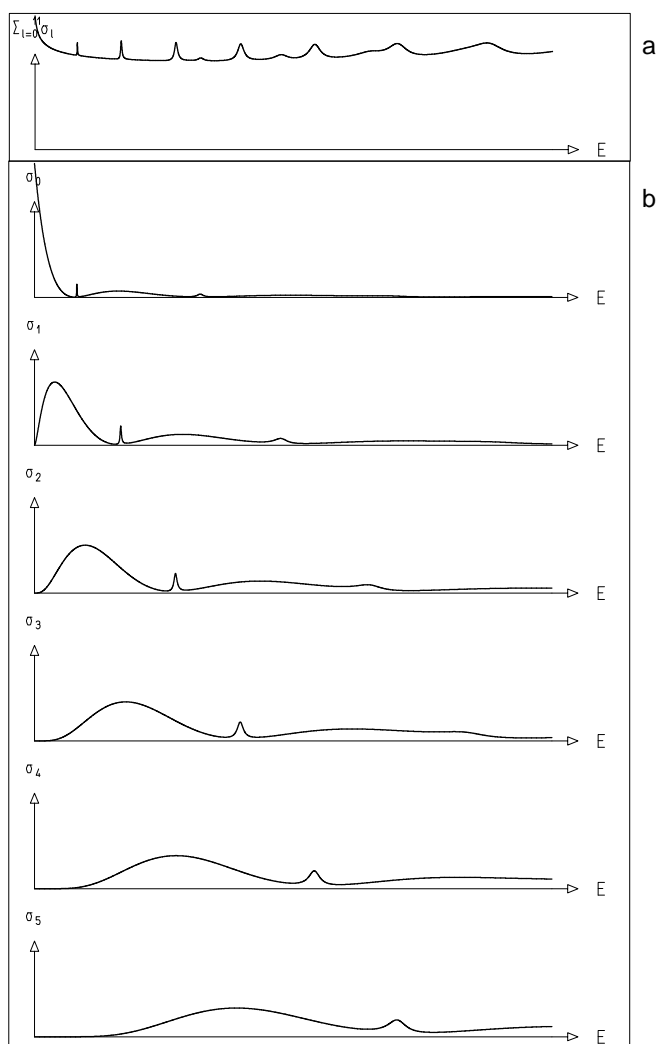


Fig. 15.10. Energy dependence of the radial wave function  $R_\ell(k, r)$  for scattering by an attractive square-well potential. The form of the potential is indicated by the long-dash line, the wave energy by the short-dash line, which also serves as zero line for the wave function. Whereas  $R_0$ ,  $R_1$ , and  $R_2$  change very little within the potential region, near the energy  $E_{\text{res}}$  the wave function  $R_3$  of the resonant partial wave develops a very pronounced maximum. Outside the potential region all wave functions show trivial shortening of the wavelength with growing energy.



**Fig. 15.11.** Bound states and resonances of an attractive square-well potential for angular-momentum quantum number  $\ell = 3$ . The potential wells have constant fixed widths but different depths. The potential  $V(r)$  is shown as a long-dash line. The effective potential is also shown. (a) For a rather deep potential well there are two bound states with negative energies indicated by the horizontal short-dash lines. The lower bound state has no radial nodes; the second has one node. (b) A somewhat shallower well has only one bound state but it does have a resonance. The resonance energy corresponds to the horizontal line of positive energy. The radial wave function  $R_3(k_{\text{res}}^{(2)}, r)$  has one node in the potential region, just as the second bound state in part a has. (c) This potential well has only one bound state. (d) The bound state in part c now reappears as a resonance. Its wave function is  $R_3(k_{\text{res}}^{(1)}, r)$ . The resonance is the same as that in Figures 15.3 through 15.10.



**Fig. 15.12.** Energy dependence of the partial cross sections  $\sigma_\ell(E)$  and of the total cross section  $\sigma_{\text{tot}}(E)$ , which is approximated by the sum over the first few partial cross sections. Resonances for the different partial waves are visible as maxima in  $\sigma_\ell$  and  $\sigma_{\text{tot}}$ . The maxima are rather sharp for the first resonance and broader for the second. The resonances shift systematically to higher energies as angular-momentum quantum number  $\ell$  increases. The energy ranges from  $E = 0$  to  $E = 2V_0$ .

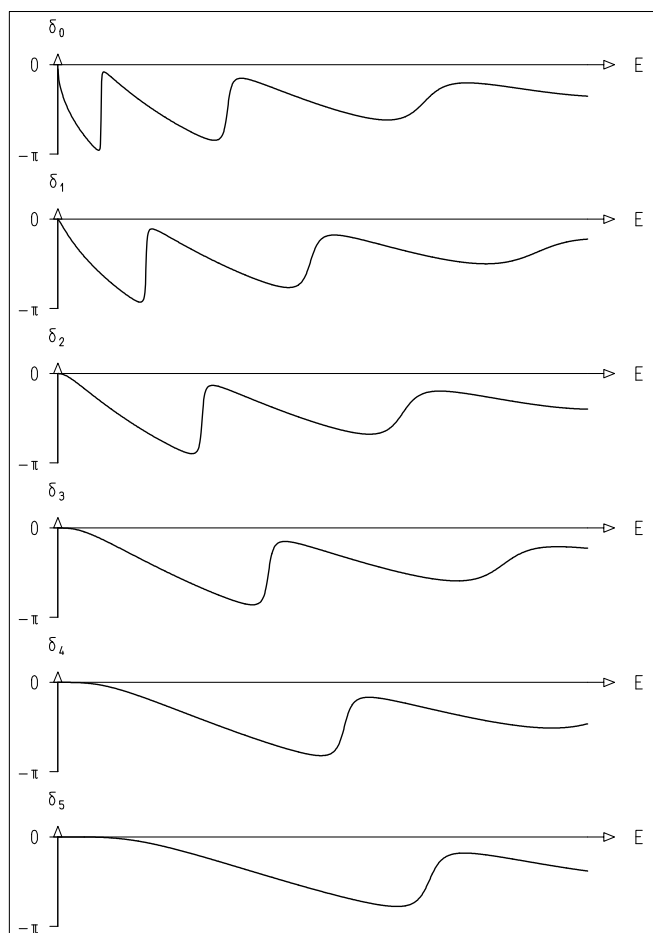


**Fig. 15.13.** Energy dependence of the phase shifts  $\delta_\ell(E)$ . At a resonance energy the corresponding phase shift rises steeply and passes through  $-\pi/2$ . See also Figure 15.14. The energy ranges from  $E = 0$  to  $E = 2V_0$ .

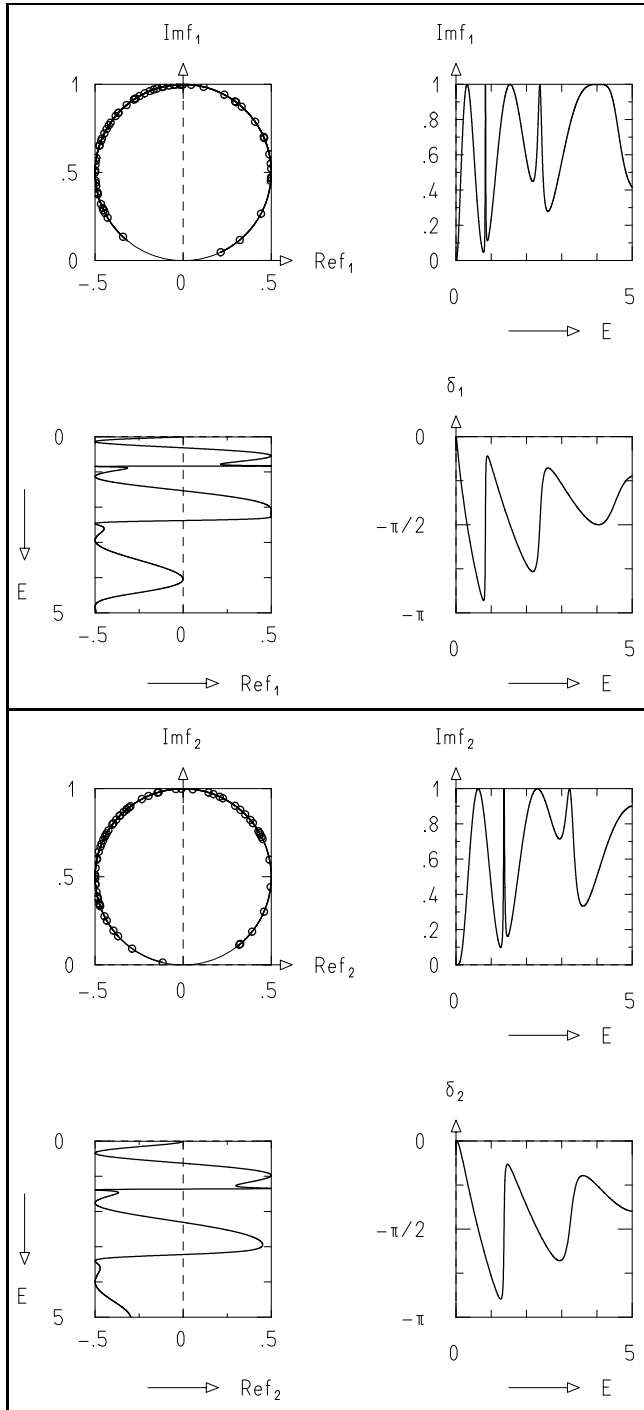


**Fig. 15.14.** Argand diagrams for the complex partial scattering amplitudes  $f_1(E)$  and  $f_2(E)$  for scattering by a repulsive shell. As in Figures 15.12 and 15.13, the energy ranges from  $E = 0$  to  $E = 2V_0$ . The resonances have a swift counterclockwise motion of  $f_\ell$  through the point  $(0, 1)$  in the complex plane, and the characteristic resonance patterns in  $\text{Im} f_\ell(E)$ ,  $\text{Re} f_\ell(E)$ , and  $\delta_\ell(E)$  already familiar from Figure 15.8 (bottom). Because of the shell structure of the potential, there are now more resonances.

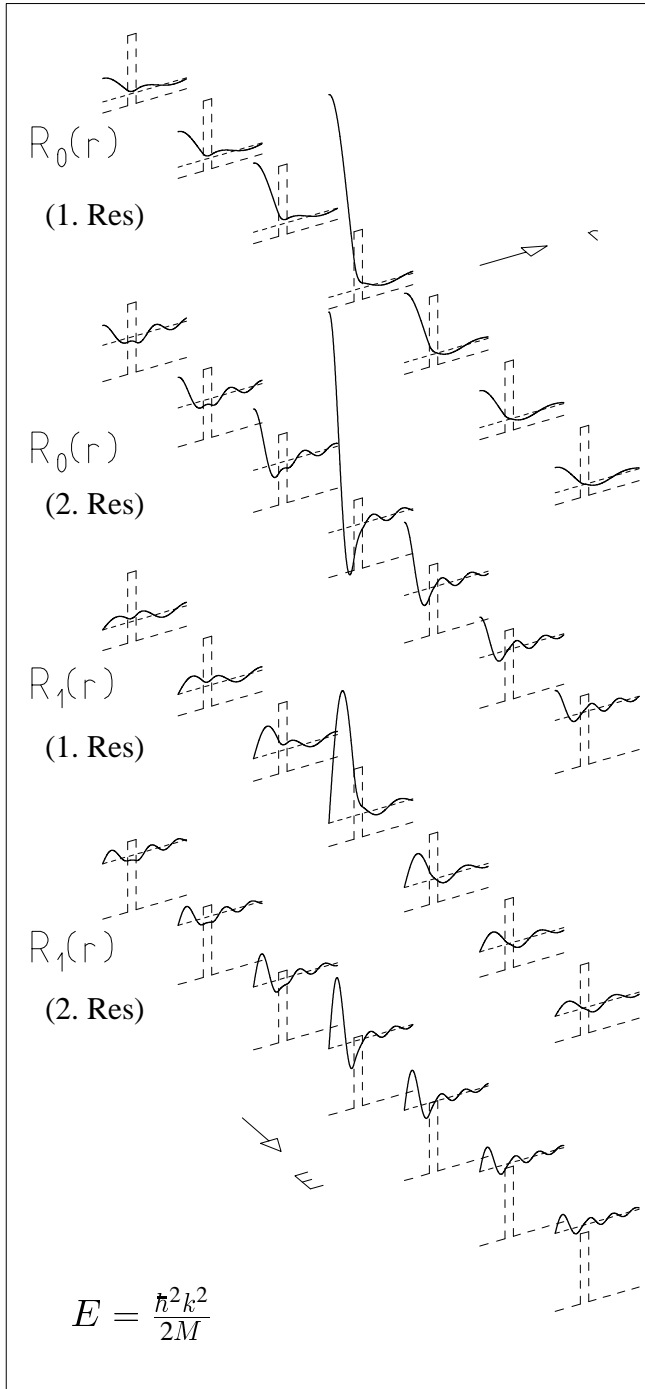


**Fig. 15.15.** Energy dependence of the radial wave functions  $R_\ell(k, r)$  within restricted energy intervals surrounding the resonances in  $\ell = 0$  and in  $\ell = 1$  for scattering by a repulsive shell. The form  $V(r)$  of the potential is indicated by the long-dash line, the energy  $E$  of the wave by the short-dash line. The middle diagram of each series corresponds to the resonance energy. The wave functions  $R_\ell(k_{\text{res}}, r)$  shown in these middle diagrams display no node and one node inside the shell for the first and second resonance, respectively.

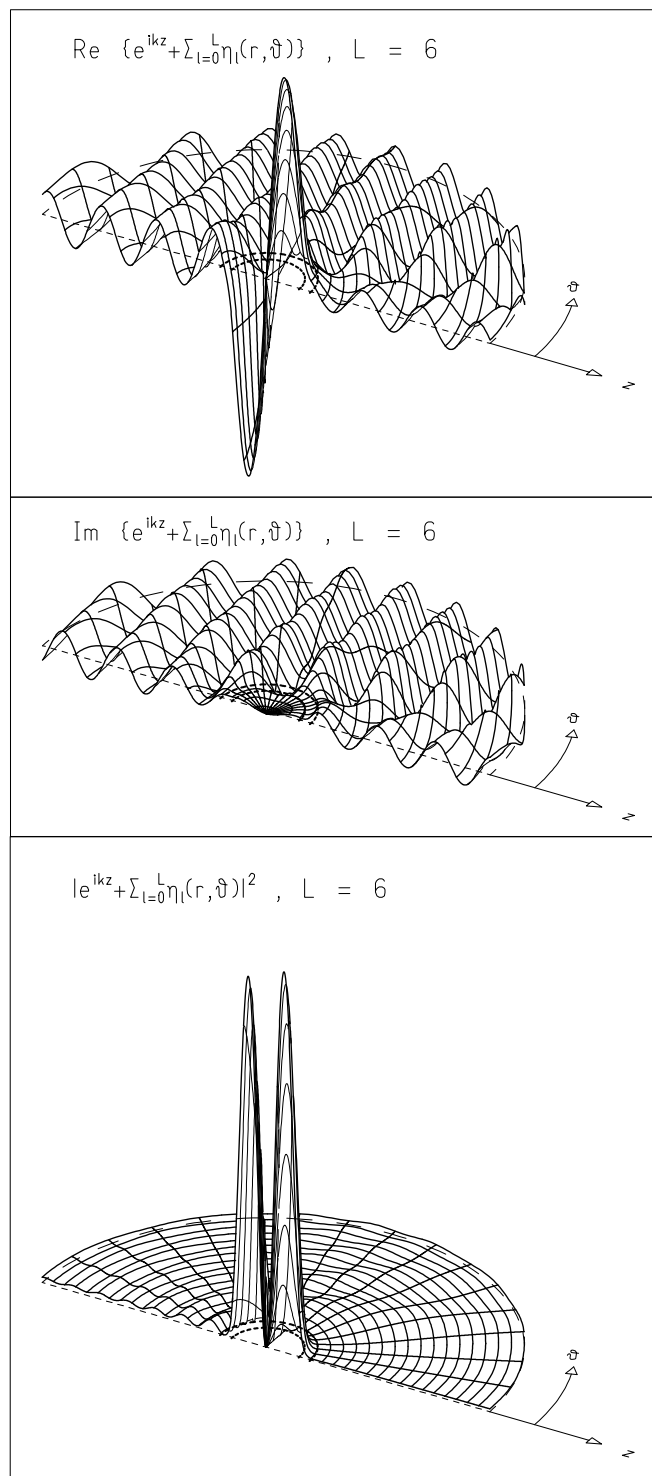


Fig. 15.16. Wave functions  $\varphi_{\mathbf{k}}^{(+)}$  for the scattering of a plane wave incident along the  $z$  direction by a repulsive shell. The energy is that of the first resonance in partial wave  $\ell = 1$ . The two half-circles near the center indicate the inner and outer boundaries of the spherical potential shell.



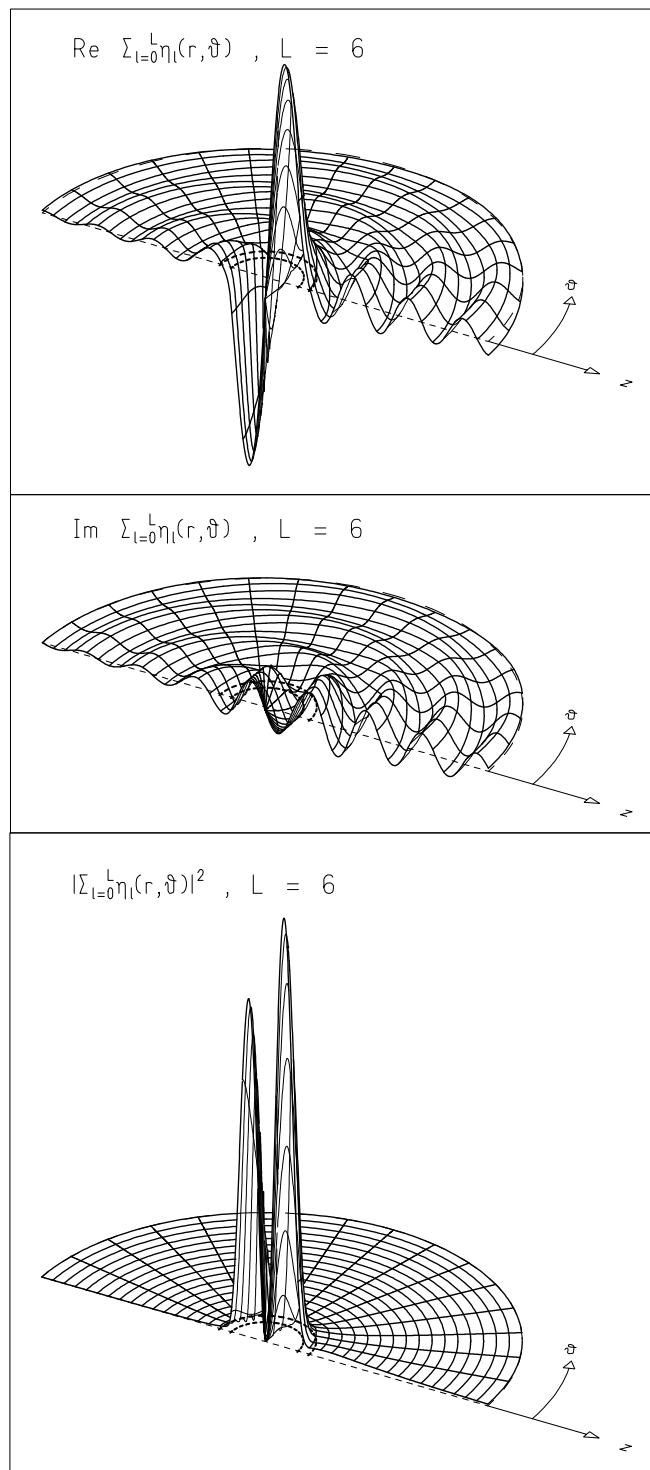
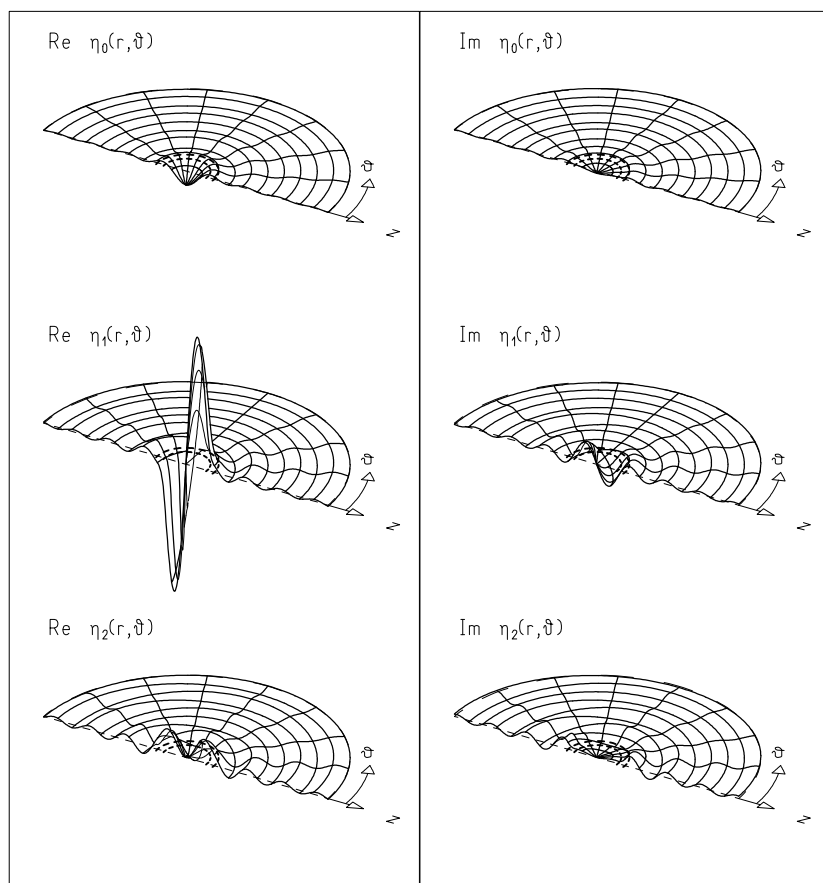
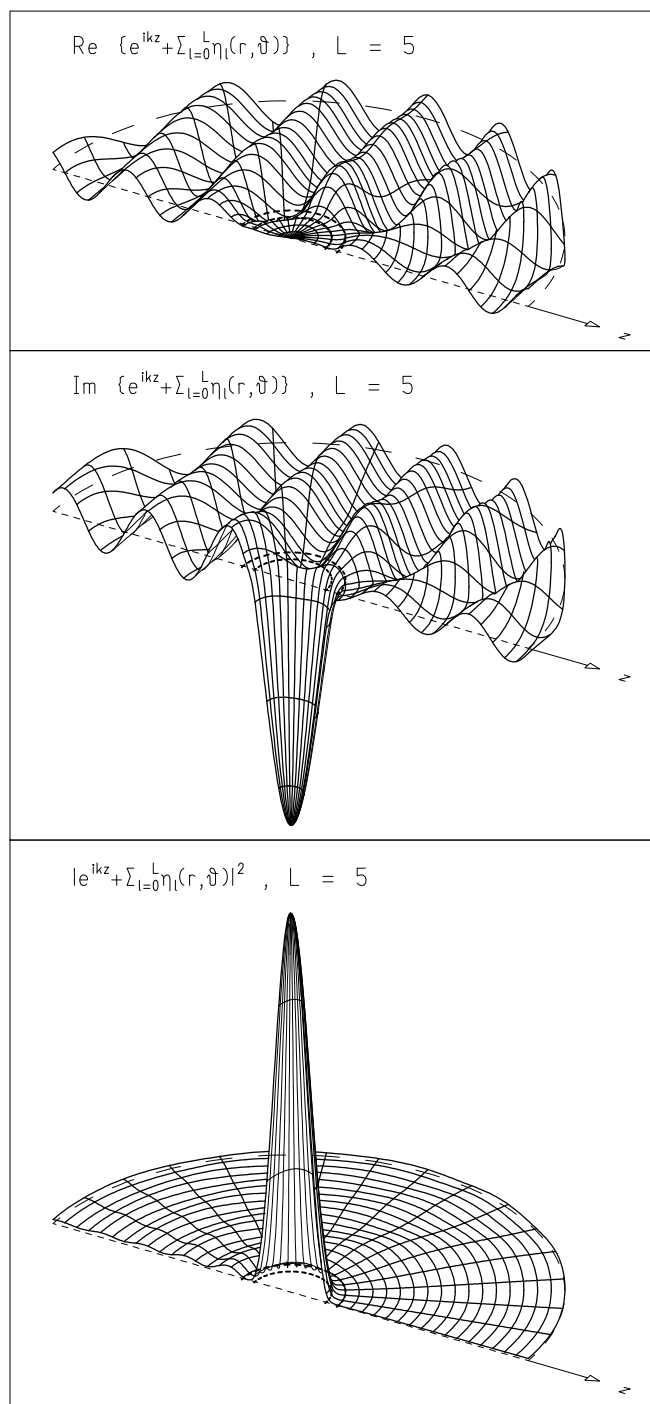


Fig. 15.17. The scattered spherical wave  $\eta_k$  resulting from the scattering of a plane wave incident along the  $z$  direction by a repulsive shell. The energy is that of the first resonance in partial wave  $\ell = 1$ .



**Fig. 15.18.** Scattered partial waves  $\eta_\ell$ ,  $\ell = 0, 1, 2$ , resulting from the scattering of a plane wave incident along the  $z$  direction by a repulsive shell. The partial wave  $\eta_1$  has its first resonance at this particular energy of the incident plane wave.



**Fig. 15.19.** Wave function  $\varphi_{\mathbf{k}}^{(+)}$ , for the first resonance in  $\ell = 0$  produced by the scattering of a plane wave incident along the  $z$  direction by a repulsive potential shell.

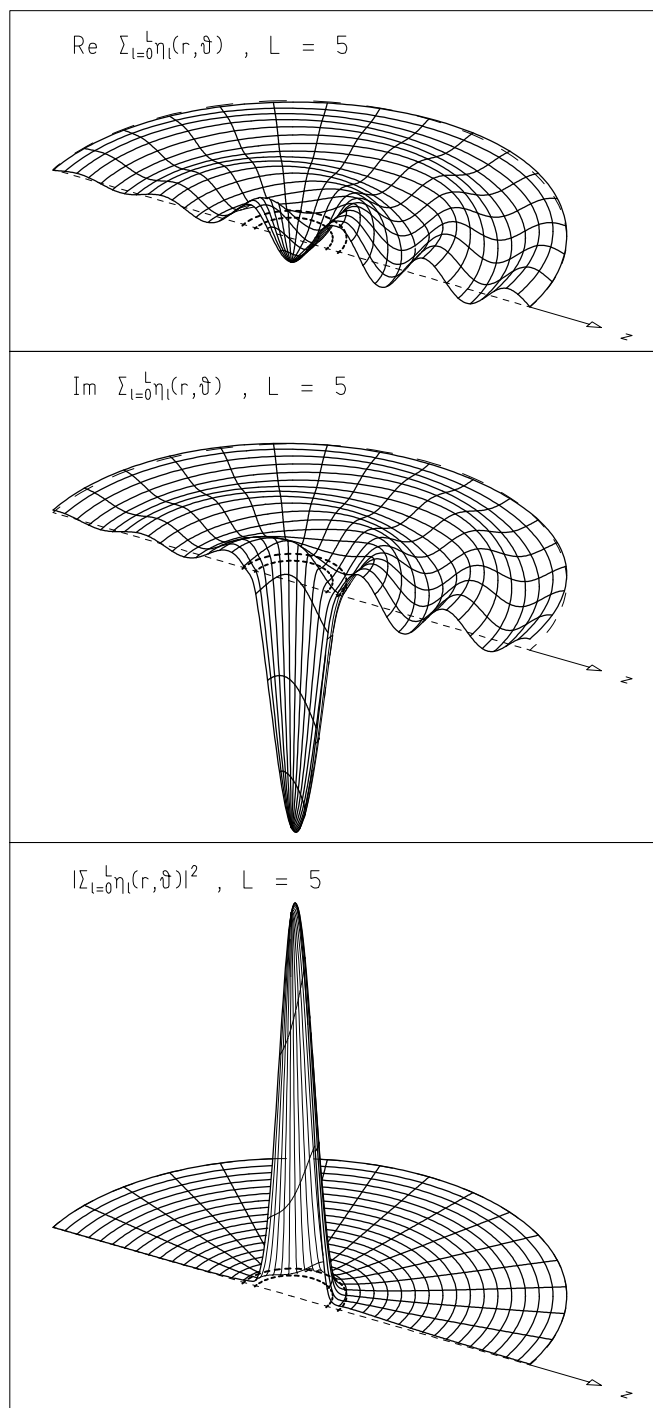


**Fig. 15.20.** Scattered spherical wave  $\eta_k$  for the first resonance in  $\ell = 0$  produced by the scattering of a plane wave incident along the  $z$  direction by a repulsive potential shell.

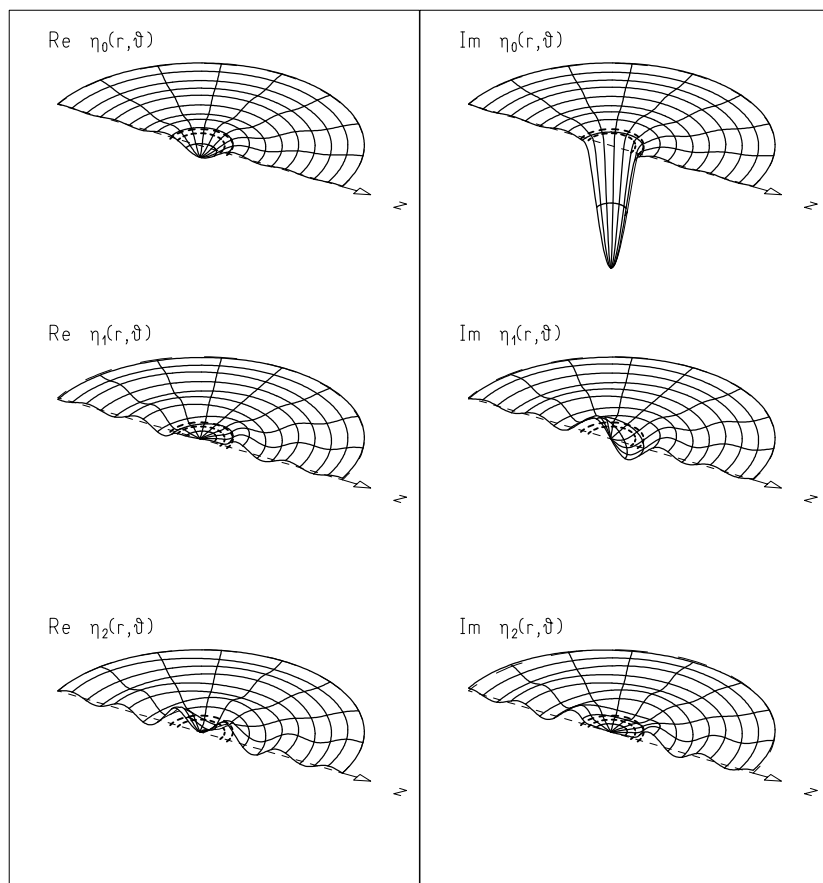


**Fig. 15.21.** Scattered partial waves  $\eta_\ell$  for the first resonance in  $\ell = 0$  produced by the scattering of a plane wave incident along the  $z$  direction by a repulsive potential shell.